Excited State Decay Pathways of Molecular Rotors: Twisted Intermediate or Conical Intersection?

Tomislav Suhina,[†,‡] Saeed Amirjalayer,[¶] Benedetta Mennucci,[§] Sander Woutersen,[*,†] Michiel Hilbers,[†] Daniel Bonn,[‡] and Albert M. Brouwer[*,†]

†*van 't Hoff Institute for Molecular Sciences, University of Amsterdam, PO Box 94157, 1090 GD Amsterdam, The Netherlands*

‡*van der Waals-Zeeman Institute, Institute of Physics, University of Amsterdam, PO Box 94485, 1090 GL Amsterdam, The Netherlands*

¶*Center for Nanotechnology (CeNTech) and Physical Institute, University of Münster, Heisenbergstrasse 11, 48149 Münster, Germany*

§*Dipartimento di Chimica e Chimica Industriale, University of Pisa, via G. Moruzzi 13, 56124 Pisa, Italy*

E-mail: s.woutersen@uva.nl; a.m.brouwer@uva.nl

Contents

Steady state absorption and emission spectra

Steady state spectra of **1** in a range of solvents are shown in Figures S1- S5. Spectra are all scaled to the same maximum in intensity/absorbance.

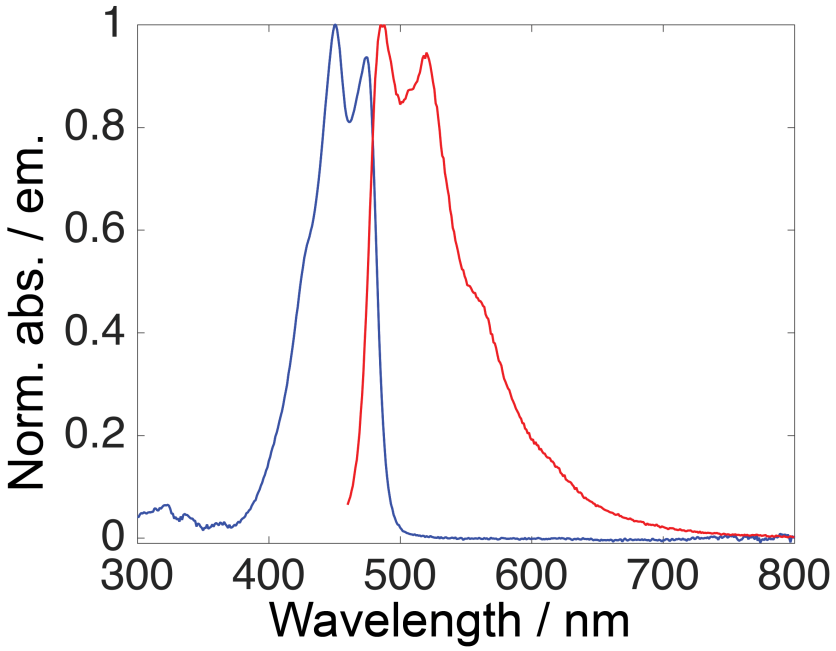

Figure S1: Absorption and emission spectra of **1** in hexane.

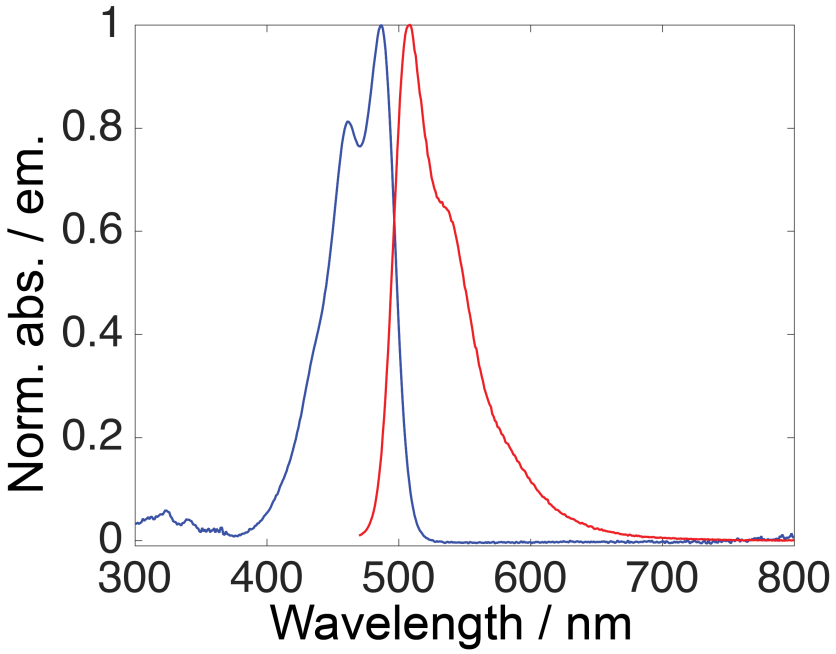

Figure S2: Absorption and emission spectra of **1** in toluene.

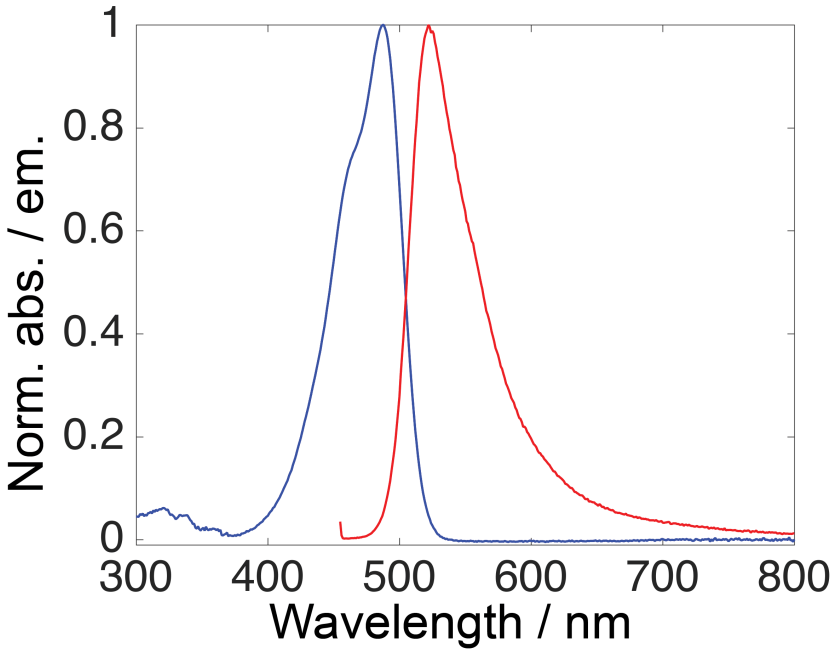

Figure S3: Absorption and emission spectra of **1** in EtOAc.

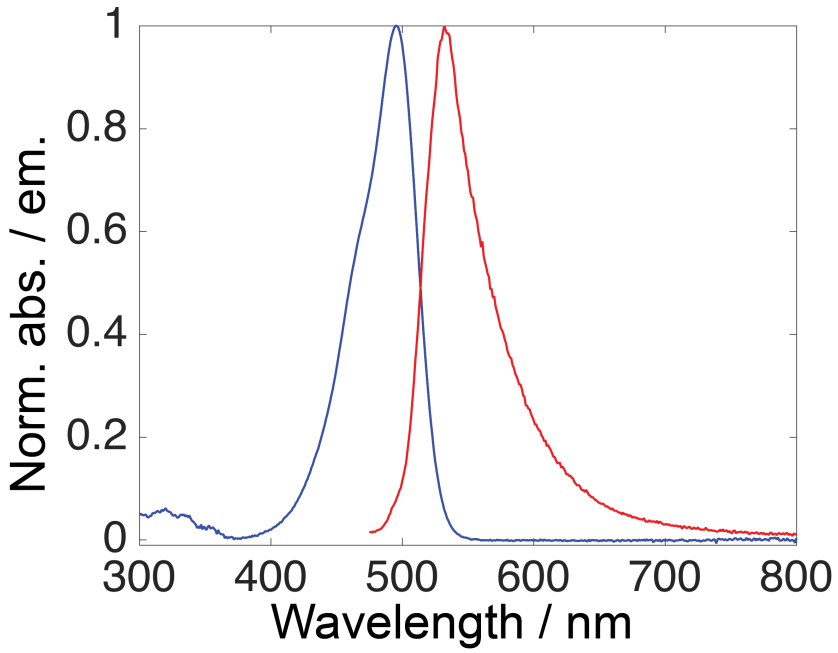

Figure S4: Absorption and emission spectra of **1** in MeCN.

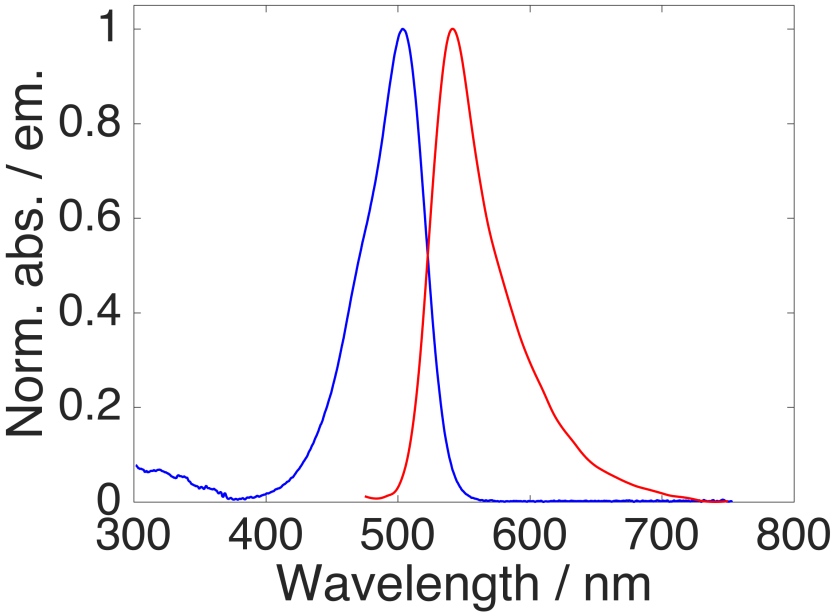

Figure S5: Absorption and emission spectra of **1** in DMSO.

Solvatochromism

A common way of describing solvatochromism is based on the Lippert-Mataga equation[1] (LM), in which the Stokes shifts are expressed as a function of solvent orientation polar-

ization.[2] In its commonly used form, the LM equation ignores specific interactions, and only considers the polarization induced in the solvent by the fixed ground and excited state dipoles. The polarizability of the solute is taken into account in the polarizable point dipole dielectric continuum model, where the solvent polarizability function is replaced with $d_c(x)$ (see Equations 1, 2 and 3; for more detailed model description see ref. 3–5). In this model, c is a parameter related to solute polarizability α and it can vary between c=0 (non-polarizable limit in which case Eq. 2 assumes solvent polarizability expression Δf from LM analogous to Eq. 3) and c=0.5 which is another common choice and results in $d_c(x) = (x-1)/(x+2)$. For **1** we use the value of 0.25 which was obtained from the relation c = α/a^3, where α = 278.93 bohr^3 represents the solute polarizability and a =10.44 bohr^3 represents an effective cavity radius. These values were obtained from DFT calculations (CAM-B3LYP/6-31G+(d). $h\nu^0_{abs}$ and $h\nu^0_{em}$ represent energies of absorption and emission maxima in vacuum, respectively. Details are presented in Table S1. The linear fit of the Stokes shift vs. the modified polarizability function (Figure S6) yields $\Delta\mu$ = 5.8 ± 0.9 D. With the slope of the plot in cm^{-1} and radius in Angstroms, $\Delta\mu$ can be calculated from eq. 4.

$$\nu_{abs} - \nu_{em} = \frac{2}{hc}[d_c(\epsilon) - d_c(n^2)]\frac{\Delta\mu^2_{S_1-S_0}}{a^3} + h\nu^0_{abs} - h\nu^0_{em} \tag{1}$$

$$d_c(x) = \frac{d_0(x)}{1 - 2cd_0(x)} = \frac{x-1}{2(1-c)x + (1+2c)} \tag{2}$$

$$d_0(x) = \frac{x-1}{2x+1} \tag{3}$$

$$\Delta\mu = \sqrt{9.9316 \times 10^{-5} \times slope \times a^3} \tag{4}$$

Spectra were measured for a series of selected solvents with short relaxation time and which are not expected to have specific interactions with **1**.

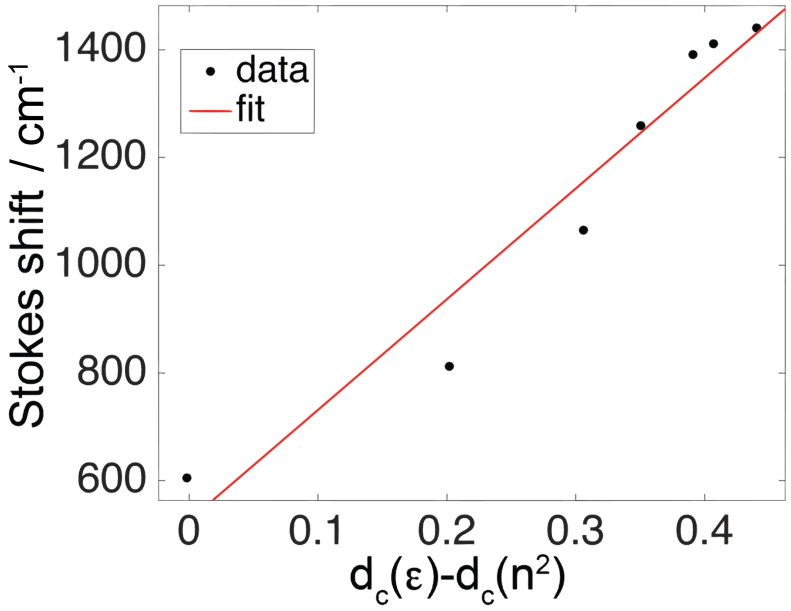

Figure S6: Stokes shifts as a function of $d_c(\epsilon)$ - $d_c(n)$ measured for **1** in hexane, chloroform, dichloromethane, benzonitrile, DMSO, acetone, and acetonitrile.

Strickler-Berg equation

Under the assumption that the electronic transition dipole moment for absorption is equal to the electronic transition dipole moment for emission ($M_{01} = M_{10}$) the Strickler-Berg relationship[6] can be used to estimate the radiative rates from the $S_0 \rightarrow S_1$ absorption band. In other words, in order to use this expression, one has to assume that the ES geometry is similar to the GS geometry. If quantum yields are known, fluorescence lifetimes can be estimated using expression 9. Expressions 7 and 8 allow for estimation of transition dipole moments. In these equations, ν are expressed in cm^{-3}, ϵ in $M^{-1}cm^{-1}$, transition dipole moments in D, and k_{rad} in s^{-1}. Results can be seen in Table S1.

$$k_{rad} = 2.88 \times 10^{-9} n^2 (\tilde{\nu}^3_{em}) \int_{S1} \frac{\epsilon(\nu)}{\nu} d\nu \tag{5}$$

$$\tilde{\nu}^3 = \frac{\int F(\nu) d\nu}{\int F(\nu) \nu^{-3} d\nu} \tag{6}$$

$$M_{01} = 9.58 \times 10^{-2} \sqrt{\frac{1}{n} \int_{S_1} \frac{\epsilon(\nu)}{\nu} d\nu} \tag{7}$$

$$M_{10} = 1.786 \times 10^{3} \sqrt{\frac{k_{rad}}{n^3 \tilde{\nu}^3}} \tag{8}$$

$$\tau_{pred} = \Phi_f / k_{rad} \tag{9}$$

Table S1: Results obtained using the Strickler-Berg equation.

Solvent	Φ_f/%	$k_{rad} \times 10^8/s^{-1}$	τ_{pred}/ps	$M_{01} = M_{10}/D$	$\epsilon_{max,abs}$	$\lambda_{max,abs}$/nm	$\lambda_{max,em}$/nm
hexane	∼0.6	2.8	∼ 20	7.33	59900	474*	486**
toluene	5.0	3.1	160	6.74	62200	487	509
EtOAc	2.9	2.8	46	7.85	68000	488	522
MeCN	∼0.3	2.8	11	8.10	75800	495	532
DMSO	∼0.5	3.0	17	7.24	76000	504	541

* lowest energy peak; ** highest energy peak

As can be seen from Table S1, k_{rad} values are consistent within experimental uncertainties in the solvents used and $M_{01} = M_{10}$. In addition, predicted fluorescence lifetimes show good agreement with the values obtained by time-resolved measurements in toluene, EtOAc and DMSO; thus indicating that fluorescence emission indeed occurs only from the planar LE state.

Steady state fluorescence at different temperatures

As discussed in the main text, fluorescence deactivation of **1** in non-polar solvents occurs through rotation around the dicyanomethylene double bond (γ). As the reaction coordinate progresses, PES of S_1 and S_0 suddenly come very close together and calculated oscillator strength values decrease abruptly, thus strongly indicating the presence of a conical intersection. Since this twist presents the major deactivation pathway for **1** in these solvents, the reaction rate for non radiative decay can be expressed in a linearized Arrhenius form and yield an estimation of the energy barriers leading to fluorescence deactivation in these two solvents.

In order to asses the activation barrier leading to the conical intersection (γ twist), we measured fluorescence intensities as a function of temperature in non-polar solvents toluene and hexane (in which we found no indication of TICT formation). In these solvents (provided that intensities are measured over a reasonable range of temperatures) dielectric properties are not expected to change considerably, allowing us to estimate γ twist energy barrier with relatively small uncertainties and compare their values with results obtained from TD-DFT calculations (see below).The fluorescence deactivation rate can be expressed in the terms of fluorescence intensity, which is directly proportional to Φ_f. Fluorescence quantum yield can be expressed by equation 10, which can be rearranged to yield equation 11. If we assume that k_{rad} remains constant over the measured temperature range, then fluorescence intensity will be inversely proportional to the twisting rate ($k_\gamma = k_{nr}$).

$$\Phi_f = \frac{k_{rad}}{k_{rad} + k_{nr}} \tag{10}$$

$$k_\gamma = \frac{k_{rad}}{\Phi_f} - k_{rad} = k_{rad}(\frac{1}{\Phi_f} - 1) \tag{11}$$

By taking the Förster-Hoffmann equation[7] into account (see eq. 12), the effect of viscosity change on fluorescence can be accounted for in Arrhenius expression and Eq 13 is obtained.

$$\Phi_f = constant \times \eta^\alpha \tag{12}$$

$$ln(k_\gamma) = constant_1 - \frac{E_a}{RT} - constant_2 - \alpha \times ln(\eta(T)) \tag{13}$$

Since the viscosities of hexane and toluene show Arrhenius-type behavior and thus follow equation 14,[8] we can express the equation 13 in the form presented in equation 15.

$$ln(\eta) = \frac{B}{RT} + constant \tag{14}$$

$$ln(k_\gamma) = constant - \frac{E_a}{RT} - \alpha \times ln(a \times e^{\frac{B}{RT}}) = constant - \frac{E_a}{RT} - \alpha \times (\frac{B}{RT}) \qquad (15)$$

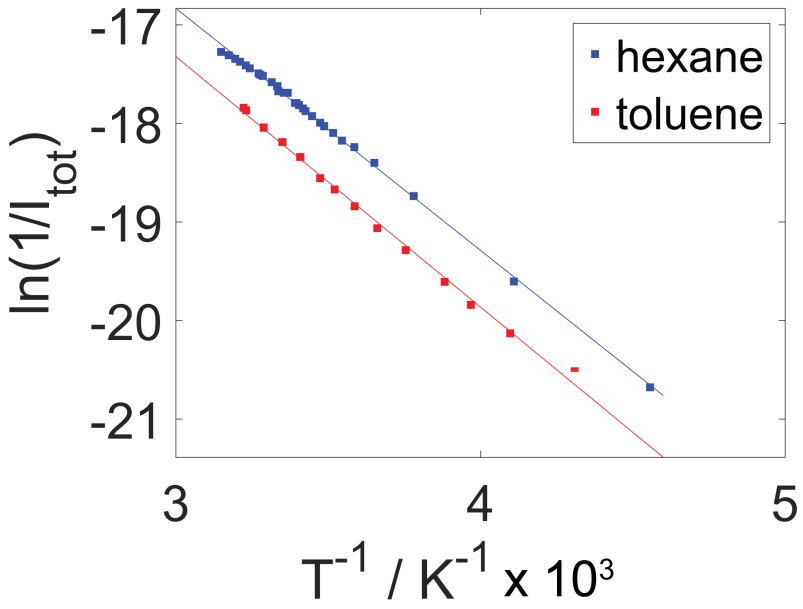

Figure S7: Natural logarithm of inverse total intensity (corrected for viscosity response) as a function of inverse temperature for **1** in hexane and toluene.

We assume the value of Förster-Hoffmann (FH) pre-exponential factor $\alpha = 2/3$ based on our previous work.[9] We note, however, that this value was obtained by measuring fluorescence response to viscosity in polar solvent (MeCN) for acid analogue of **1** (**2**, see main text), and FH pre-exponential factors might differ in non-polar hexane and toluene. Although this might introduce some error, this error is significantly smaller than ignoring the viscosity effect completely. Viscosity barriers (B) for hexane and toluene are obtained by fitting the experimental viscosity data[10] to equation 14. These parameters are used in Equation 15, where $\ln(k_\gamma)$ is replaced with $\ln(1/I_{tot})$ (because of Eq 11).

Linear fit produces activation energy barriers for γ isomerization of 3.59 $\pm$ 0.07 and 3.62 $\pm$ 0.19 kcal/mol for hexane and toluene, respectively. One needs to keep in mind that these barriers are overestimated, since the barrier response to the change in dielectric constant can't be determined with the currently available data.

TD-DFT calculations

Calculations shown in the main text were performed on a model molecule **1a**, where dihexyl chains were replaced with methyl groups in order to reduce calculation costs, (Figure S8) with CAM-B3LYP/6-31+G(d) level of theory.[11] Although this functional is known to overestimate vertical excitation energies, it provides good qualitative description of systems with significant charge-transfer character.[12] To further validate the results, PES scans were repeated with ωB97DX/6-31G(d),[13] but the obtained trends were the same. Solvent effects were included through the Integral Equation Formalism (IEF)[14] version of the Polarizable Continuum Model (PCM).[15] Relaxed excited state PESs have been obtained assuming a complete relaxation of the solvent polarization. To account for a proper response of the solvent, a State-Specific correction has been introduced for each point of the PESs through the cLR formulation.[16] All calculations have been done with a locally modified version of Gaussian '09 software.[17]

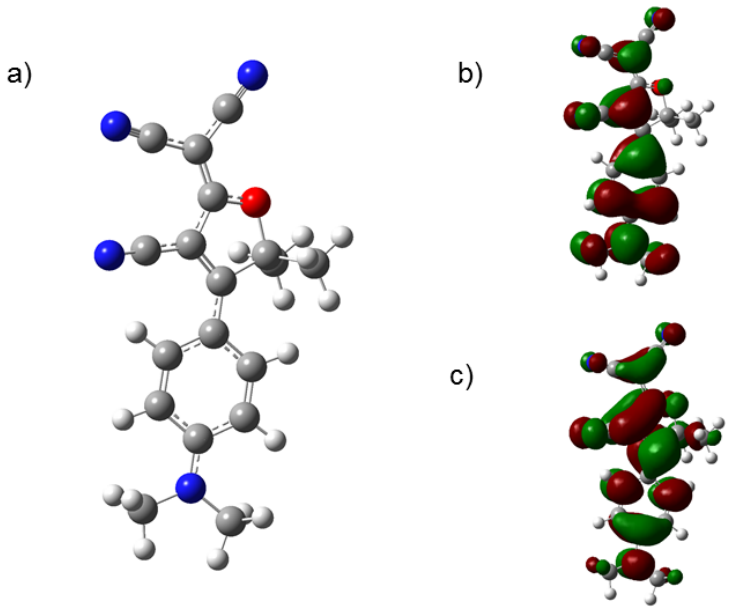

Figure S8: a) Optimized ground state molecular geometry of **1a** in DMSO; b) HOMO c) LUMO

Figure S8 shows the relaxed ground state geometry obtained for **1a** in DMSO. Geometries

obtained for **1a** in vacuum and toluene are similar to the one shown in Figure S8 with small variations in dihedral angles between benzene-furan ring and furan-C-CN planes. These small variations in structure are accompanied by increase in ground state dipole moments from vacuum (16.6 D), through toluene (20.0 D) to DMSO (24.1 D). The dipole moments further increase in the excited state (to 18.0 D, 23.7 D and 29.5 D, respectively), which is indicated by more pronounced electron density on the acceptor part in LUMO. Calculated $\Delta\mu$ are somewhat lower (2.0, 3.7 and 5.4 D for vacuum, toluene and DMSO respectively) than the experimentally obtained value of $\sim$5.8 D.

While performing the excited PES scans, we found three minima (see Figure S9). One minimum is associated with a planar structure (Figure S9a, another one with the δ twisted (Figure S9c and the final one with the β twisted geometry (Figure S9).

Planar locally excited (LE) state structures do not significantly differ from the ground state geometries. There are, however, small differences from one solvent to another. In vacuum, the phenyl-furan dihedral angle (β) changes from 16.5 in the GS to 9.4 degrees in the first ES. At the same time, the furan-C-CN dihedral (γ) changes from -0.6 to -5.7. In DMSO, the β dihedral increases from 9.5 to 18.4 degrees, while γ changes from -0.9 to -3.1 degrees going from the ground to the first ES. For both toluene and DMSO, twisting around β bond is accompanied by a large increase in the dipole moment (23.7$\rightarrow$33.7 D and 29.5.1$\rightarrow$38.8 D, respectively). Polar solvents lower the energy barrier leading to the twisted state ($\sim$3.7 kcal/mol in vacuum, $\sim$1.3 kcal/mol in toluene, $\sim$0.1 kcal/mol in DMSO). On the other hand, twisting about the γ bond causes a remarkable decrease in the calculated ES dipole moments (23.7$\rightarrow$12.4 D and 29.5$\rightarrow$13.3 D, in toluene and DMSO, respectively). An abrupt drop in oscillator strength is also observed while performing a scan around γ. The accompanying energy barrier that needs to be overcome in order to perform this twist is $\sim$3.1 kcal/mol in toluene and 5.8 kcal/mol in DMSO.

These findings indicate two important things: 1) twisting about β seems not to lead to conical intersection, but to the TICT state as a local minimum. This state is more stabi-

lized by polar solvents, and since the dipole moment gradually increases as twist proceeds, the activation barrier which needs to be overcome to reach this state becomes lower with increasing solvent polarity. This is accompanied by a gradual decrease in oscillator strength, indicating that the TICT state is a dark state. Our experiments show excellent agreement with this since we observed emission only from the LE state, but we could observe dark transient species in case of polar solvents. 2) Twisting about the γ bond results in an abrupt drop in oscillator strength (γ $\sim 50^o$ in toluene, $\sim 60^o$ in DMSO) and decrease of dipole moment (which explains the energy barrier difference in non-polar and polar solvents). GS and ES PESs at the same time come very close together, which is accompanied by pyramidization of the furan ring carbon connecting dicyanomethylene group with the rest of the molecule (see Figure S10). All this suggests the presence of a conical intersection between GS and ES at those coordinates which is expected to result in instantaneous relaxation to the GS. Our calculations predict the energy barrier (γ twist) to be $\sim$3.1 kcal/mol in toluene and 5.8 kcal/mol in DMSO. We stress that these results can be affected by the well-known limitations of TD-DFT in describing CI. However, a very good agreement is found with the experimental results which do not indicate formation of transient species in non-polar solvents, while a decrease in polarity (from toluene to hexane) results in a more efficient fluorescence deactivation (see main text).

Time-resolved fluorescence measurements

Time-correlated single photon counting

Examples of fluorescence decays measured for **1** in toluene, EtOAc and DMSO are shown in Figures S11, S12 and S13, respectively. In all cases, fluorescence decays were measured at multiple wavelengths and data was globally fitted in order to obtain fluorescence decay rates. The number of exponents used to obtain the fits was the smallest number that was needed to achieve reduced $\chi^2 < 1.15$. In addition, if significant increase in the fit quality

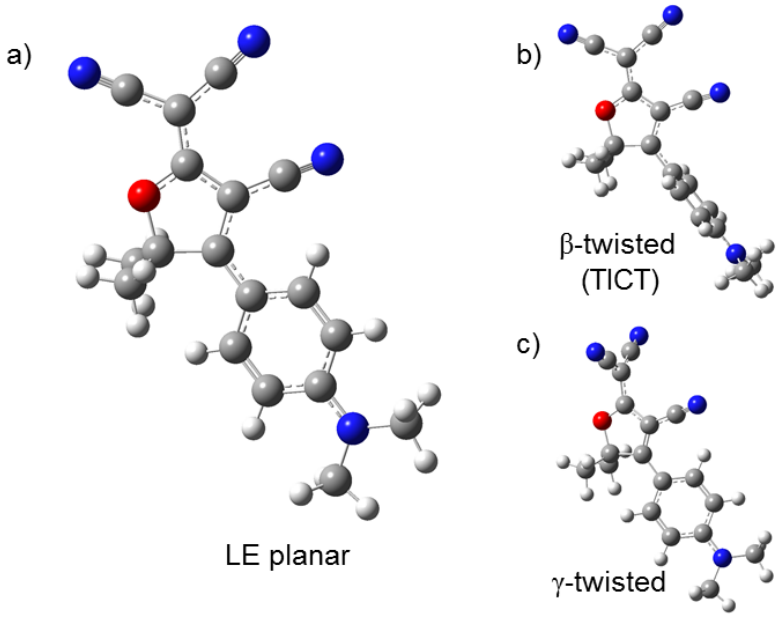

Figure S9: Three minima obtained by the PES scans of **1a** in DMSO. a) LE planar minimum; b) Minimum reached by β bond twist; c) Minimum reached by $90^o\gamma$ bond twist.

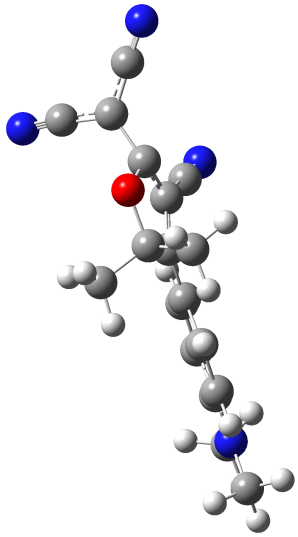

Figure S10: Structure of **1a** near conical intersection in DMSO (γ=60^o).

(χ^2 and/or residuals) was not achieved by addition of an extra component, it was excluded from the model.

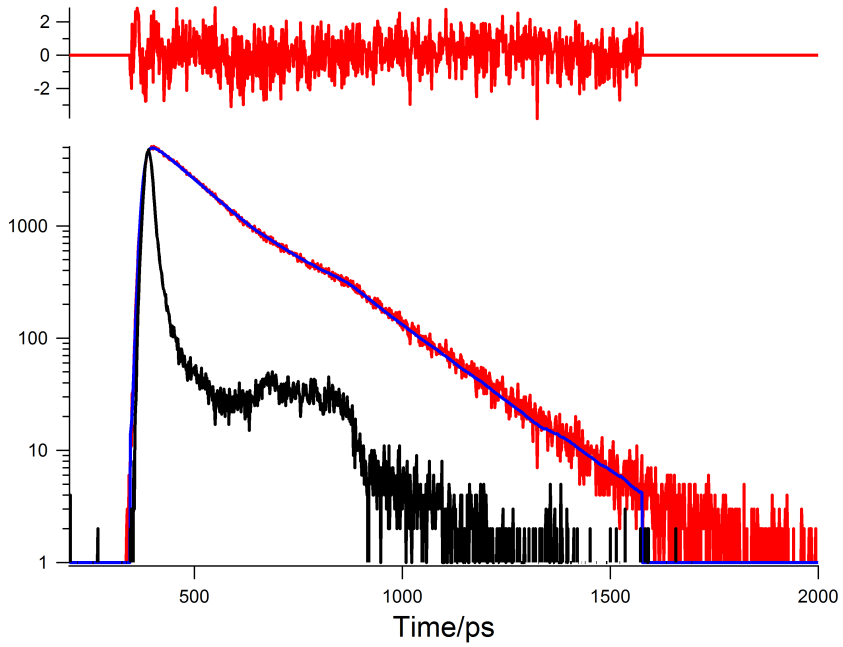

Figure S11: Fluorescence decay of **1** in toluene (λ_{exc} = 460 nm, λ_{mon} = 530 nm). Black line represents instrument response function (FWHM∼24 ps), red line represents collected data, blue line represents obtained fit.

Fluorescence decays in toluene were measured in the range 490-560 nm. Global fit of the 12 curves resulted in a single fluorescence decay time constant of 120 ps (χ^2=1.13). In case of EtOAc we had to use two exponential functions in order to obtain decent fits (χ^2 = 1.12). Time constants of 30 and 228 ps were obtained from the global fit of 6 curves. Normalized decay associated fluorescence spectra (DAFS) associated with these constants are shown in Figure S14. The two components have identical spectra, indicating that fluorescence originates from the same electronic excited state. In DMSO, fitting decays with a single time constant resulted in χ^2 values >1.4 and significant structure in the residuals. For this reason, we used a second exponent to fit 8 measured curves. This fit resulted in decay time constants of 10 and 30 ps (χ^2=1.21). Normalized DAFS associated with these time constants are shown in Figure S15. Although fit quality is not completely satisfactory, adding more components does not significantly improve the overall quality of the fit. We attribute this to

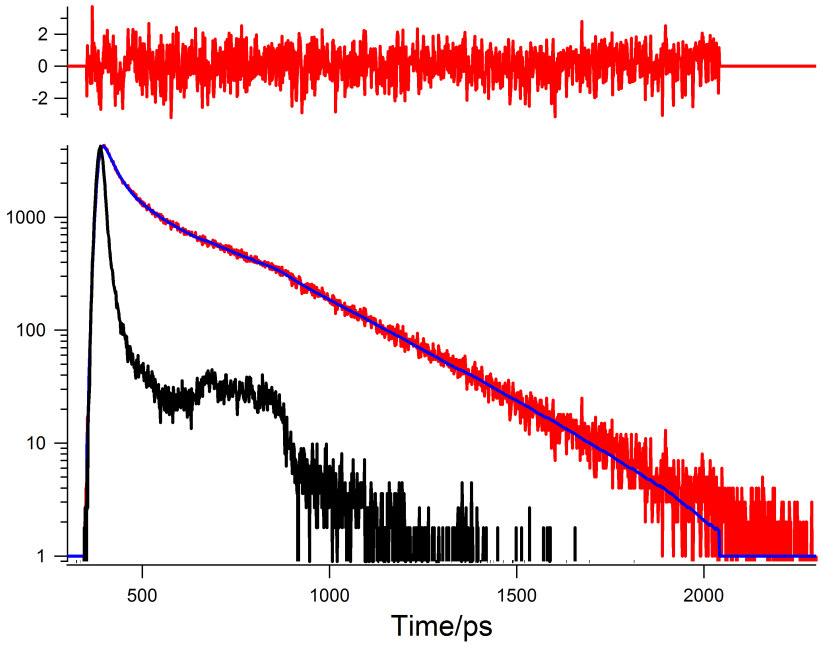

Figure S12: Fluorescence decay of **1** in EtOAc ($\lambda_{exc} = 488$ nm, $\lambda_{mon} = 530$ nm). Black line represents instrument response function (FWHM∼24 ps), red line represents collected data, blue line represents obtained fit.

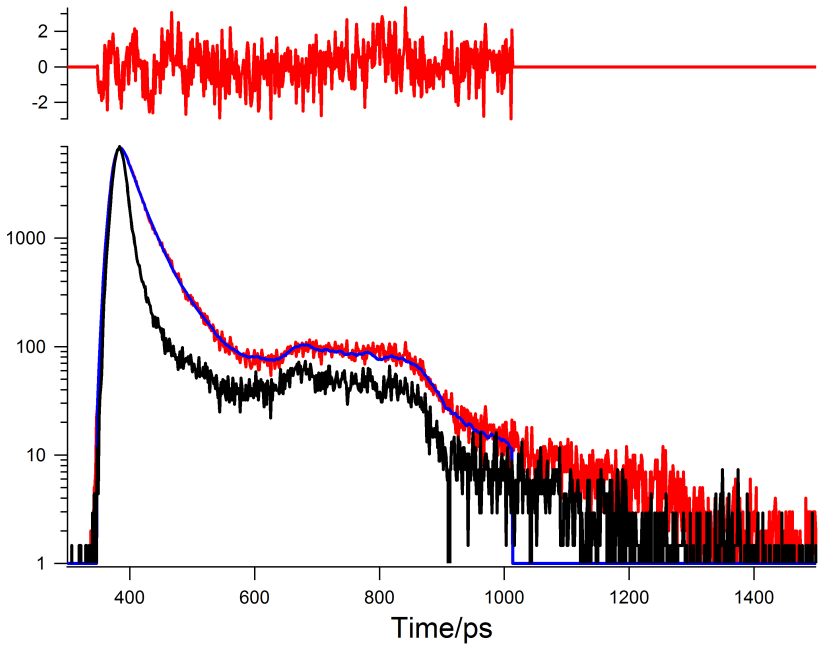

Figure S13: Fluorescence decay of **1** in DMSO ($\lambda_{exc} = 488$ nm, $\lambda_{mon} = 530$ nm). Black line represents instrument response function (FWHM∼24 ps), red line represents collected data, blue line represents obtained fit.

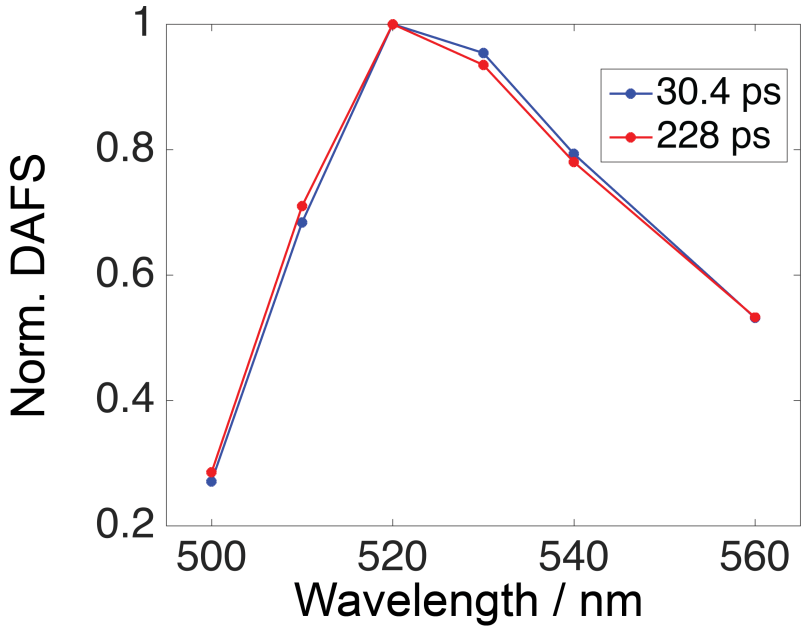

Figure S14: Reconstructed decay associated fluorescence spectra of **1** in EtOAc.

two reasons. 1) Lifetimes are very short. This means that even small artifacts in IRF and overall instrument stability will have a significant influence on the process of obtaining time constants by fitting the (exponential) function which is convolved with the IRF in order to obtain the measured decay traces. Small drifts of the IRF (and measured decays) play a more significant role as decays become shorter and as longer measurement times are needed to achieve a satisfactory number of counts per channel. More information can be found in ref. 18. 2) Competing processes, e.g. vibrational cooling and solvent relaxation, occur on a time scale of less than 10 ps. Dynamic Stokes shifts are expected to occur for molecules with pronounced charge-transfer character. This manifests itself as a spectral shift from higher to lower energies as a function of time and causes differences in fluorescence decay rates if one compares fluorescence decay measured at different wavelengths. Both 1), 2) and combination of the two have influence on both fit quality, fluorescence decay constants and even detected number of components when TCSPC histograms are fitted with exponential functions. We attribute the 10 ps component to the dynamic Stokes shift (although spectral relaxation is faster than 10 ps in DMSO)[19] and drift in our instrument which resulted from

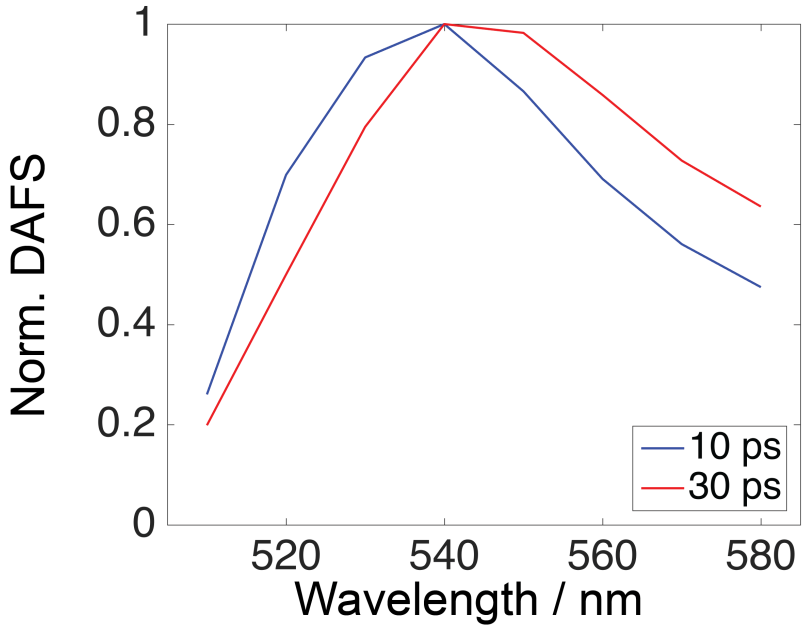

Figure S15: Reconstructed decay associated fluorescence spectra of **1** in DMSO. Shorter component is attributed to spectral relaxation and time resolution of our instrument.

long measurement time that was needed to collect a sufficient number of photons from the weakly fluorescent solution.

Variable temperature experiments in EtOAc

If we assume that **1** decays to the GS through the TICT β twisted state (T), a set of differential equations can be analytically solved for the fluorescence decay rate constants (k_1 and k_2). With our experiments it is not possible to eliminate the possibility of simultaneous deactivation through both TICT and CI (γ twist) beyond doubt, so k_{PT} might actually represent the sum of the rate constants associated with TICT state (β twisted state) formation and fluorescence deactivation through conical intersection (γ twist). This, however, seems very unlikely. If both deactivation pathways would indeed take place simultaneously, we would not expect the observed increase in quantum yields upon heating (see main text). In addition, the Arrhenius plot should strongly deviate from linearity if the two deactivation processes would be comparable in efficiency.

$$\frac{d[P]}{dt} = k_{TP}[T] - k_{PT}[P] - k_{rad}[P] = k_{TP}[T] - X[P] \tag{16}$$

$$\frac{d[T]}{dt} = k_{PT}[P] - k_{TP}[T] - k_{T0}[T] = k_{PT}[P] - Y[T] \tag{17}$$

$$[GS] = 1 - [P] - [T] \tag{18}$$

In these equations [P], [T] are concentrations of planar and twisted species, respectively. k_{PT} and k_{TP} represent the rate constants for conversion of planar to twisted, and twisted to planar species. X = $k_{rad} + k_{PT}$ and Y = $k_{TP} + k_{T0}$. In this case, initial conditions for $[P]$, $[T]$ and $[GS]$ are: $[P](t = 0) = 1$ and $T(t = 0) = [GS] = 0$. Solving this system of equations leads to analytical expressions for [P], [T] and [GS]. The time evolutions of concentration [P] can be expressed in terms of two exponential functions that contain fluorescence decay rates (k_1 and k_2) with associated amplitudes (A_1 and A_2, where A_2 = 1-A_1 due to the boundary condition [P](t=0)=1). See equations 19 and 20 for the final expressions that were obtained this way. Similar expressions have been derived in the literature to study kinetics of e.g. dimethyl amino benzonitrile.[20]

$$k_{1/2} = X + Y \pm (\sqrt{X^2 - 2XY + Y^2 + 4k_{PT}k_{TP}}) \tag{19}$$

$$A_1 = \frac{X - k_2}{k_1 - k_2}; A_2 = 1 - A_1 \tag{20}$$

Having this in mind, fitting fluorescence decays (which yields A_1, A_2, k_1 and k_2) allows us to calculate values for k_{PT}, k_{TP} and k_{T0}. Here we assume that $k_{\mathrm{rad}} = 3.8 \times 10^{-8}$ s^{-1}, based on the average lifetime obtained by measuring the fluorescence decays of **1** in PVAc matrix. Calculated rates obtained by fluorescence decay measurements over a temperature range (281.5 - 327.7K) are shown in Figure S16a and are listed in Table S2. From the

obtained rate constants, the free energy difference of P and T can be calculated from Eq. 21. The change in the free energy as a function of temperature is shown in Figure S16. As the temperature increases, the driving force for the TICT formation decreases. The reason for this is that the dielectric constant of EtOAc decreases upon temperature increase (from ~6.4 (5.5^{o}C) to ~5.4(50^{o}C). Since the TICT state is more polar than the LE state, the decrease in dielectric constant results in destabilization of the TICT state relative to the LE state upon heating.

$$\Delta G^0 = -RT \times ln(\frac{k_{PT}}{k_{TP}}) \tag{21}$$

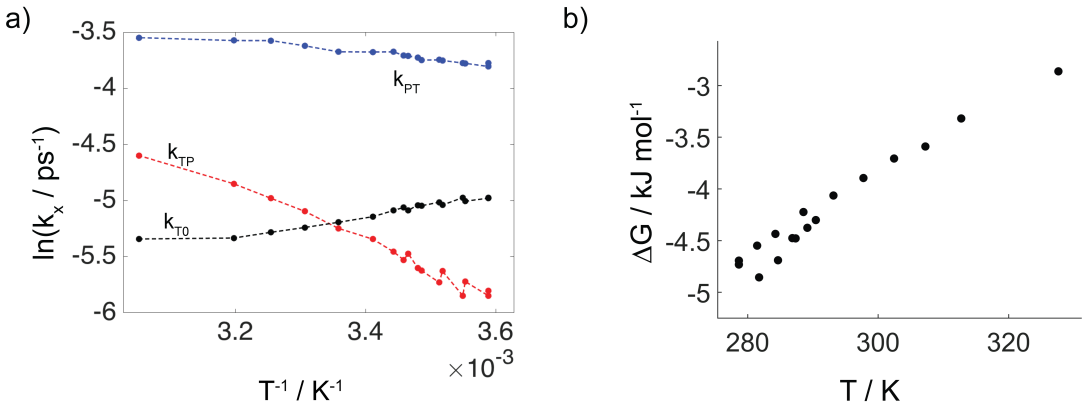

Figure S16: a) Reaction rates obtained at different temperatures for **1** in EtOAc; b) Change in free energy as a function of temperature.

Using the data presented in Table S2, one can use Van't Hoff equation (eq. 22) to estimate standard enthalpy and standard entropy change. The obtained values are ΔH^0 = -3.9± 0.15 kcal/mol and ΔS = -9.8± 0.5 cal mol^{-1}K^{-1}. The negative value of ΔS is due to increased solvation of the TICT state which causes the decrease in overall entropy.

$$ln(k_{PT}/k_{TP}) = -\frac{\Delta H^0}{RT} + \frac{\Delta S^0}{R} \tag{22}$$

Table S2: Reaction rates obtained at different temperatures for 1 in EtOAc.

T/K	$k_{pt} \times 10^{10}/\mathrm{s}^{-1}$	$k_{tp} \times 10^{9}/\mathrm{s}^{-1}$	$k_{t0} \times 10^{9}/\mathrm{s}^{-1}$
278.65	2.289	3.017	6.916
278.65	2.224	2.884	6.883
281.45	2.288	3.274	6.698
281.75	2.294	2.886	6.916
284.25	2.346	3.591	6.474
284.65	2.359	3.249	6.637
286.85	2.356	3.605	6.436
287.35	2.409	3.695	6.467
288.55	2.439	4.193	6.183
289.15	2.454	3.973	6.338
290.45	2.534	4.267	6.167
293.15	2.531	4.775	5.839
297.75	2.535	5.256	5.553
302.45	2.674	6.123	5.300
307.25	2.802	6.871	5.079
312.75	2.803	7.819	4.826
327.65	2.876	10.055	4.784

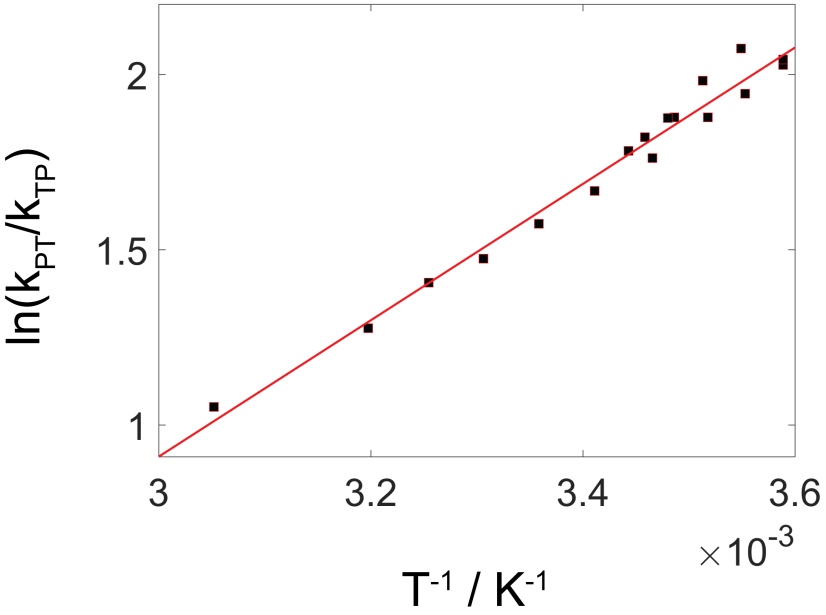

Figure S17: Natural logarithm of equilibrium constant vs the inverse temperature (Van't Hoff Plot). Obtained slope is 1945±75 J/mol with intercept of 4.92 J $\mathrm{mol}^{-1}\mathrm{K}^{-1}$

.

VIS pump mid-IR probe measurements in toluene

A partial FTIR spectrum of **1** in toluene (Figure S18) shows the bands resulting from the overlap of three -CN stretching vibrations (symmetric methylene and furan CN stretches - CN1 mode; symmetric methylene and asymmetric furan CN stretches - CN2 mode; and asymmetric methylene CN stretches - CN3 mode. The measured transient matrix ($\Delta A(\nu$, t)) is shown in Figure S19. GSB at 2200 cm^{-1} and two ESA bands centered at 2167 and 2187 cm^{-1} can be observed.

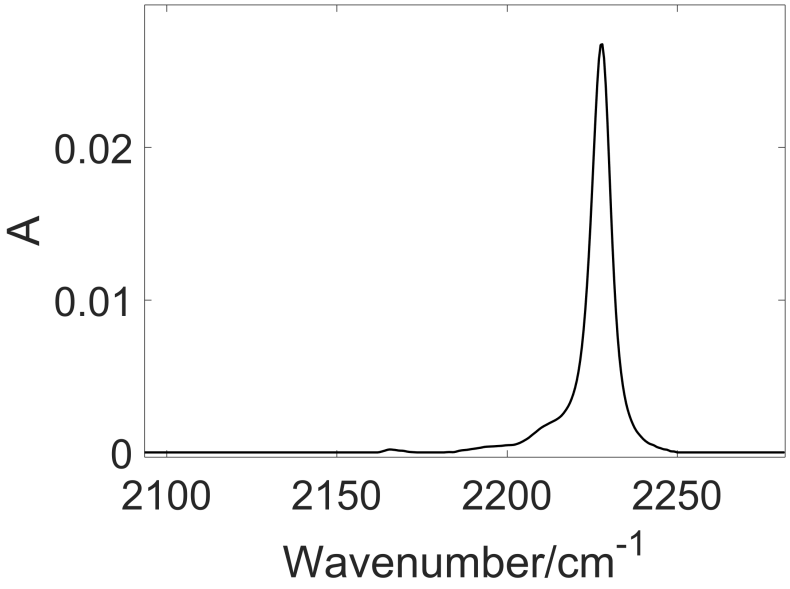

Figure S18: FTIR of **1** in toluene.

A global fit with a sequential model (LE*→LE→GS) produces two time constants of 0.8 ps and 120.2 ps. The short component is associated with solvent relaxation and vibrational cooling, while the longer one corresponds to the decay of the fluorescent planar LE state, which is in good agreement with previously discussed fluorescence measurements. The GSB signal is centered at 2220 cm^{-1} and shows single exponential recovery. Excited state absorption bands are centered at 2167 and 2187 cm^{-1} and also show single exponential decay. No other transient species can be observed, which is in excellent agreement with our assumption that emission occurs from the planar LE state which deactivates through a conical inter-

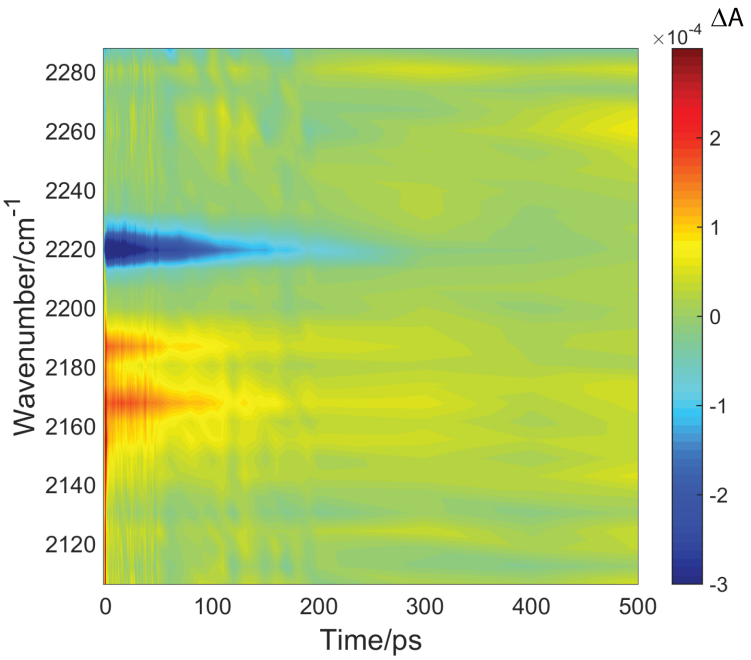

Figure S19: Transient matrix of **1** in toluene obtained by VIS-pump mid-IR probe measurements (λ_{exc}=488 nm).

section (γ twist). Representative time traces (with fits) and species associated spectra are shown in the main text.

VIS pump mid-IR probe measurements in DMSO

Partial FTIR spectra of **1** in DMSO are shown in Figure S20. Transient matrices obtained for 1 in DMSO in -C=C- and -CN stretch regions are shown in Figure S21. Since transient signals are relatively weak and artifacts were detected in the -CN stretch region (due to pump-probe interference at delays around zero), we used singular value decomposition (SVD) and filtering in order to minimize the influence of artifacts and reduce the noise level in our data. The number of components used in filtering was determined by looking at their spectral and temporal singular vectors. If no structure (of either spectral or temporal nature) was observed, SVD components were not used in filtering.[21,22] The first two singular vectors were retained. Obtained species associated spectra and time-traces (with respective fits) can be seen in the main text.

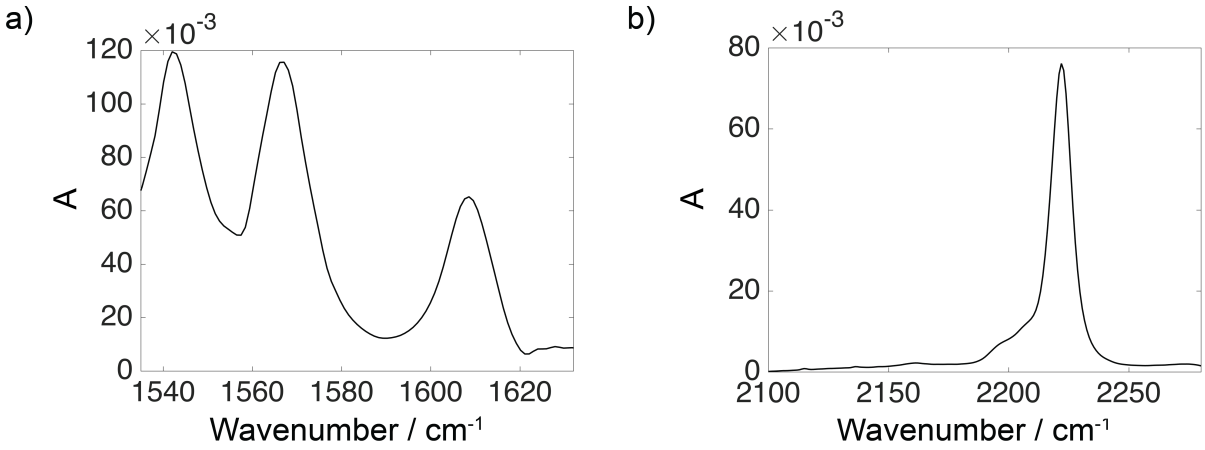

Figure S20: Partial FTIR of **1** in DMSO. a) -C=C- stretch region; b) -CN stretch region.

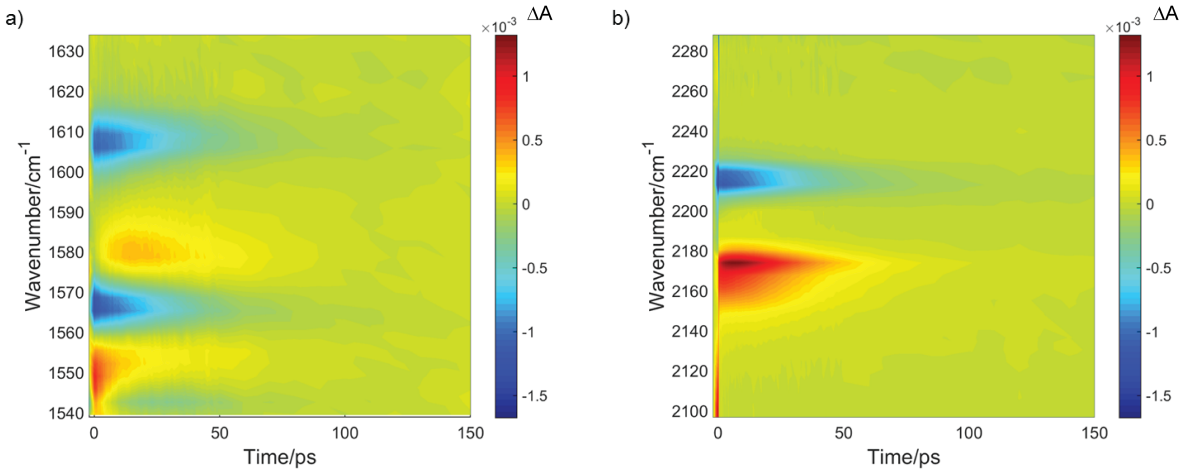

Figure S21: Transient matrix of **1** in DMSO obtained by VIS-pump mid-IR probe measurements (λ_{exc}=488 nm). a) -C=C- stretch region; b) -CN stretch region.

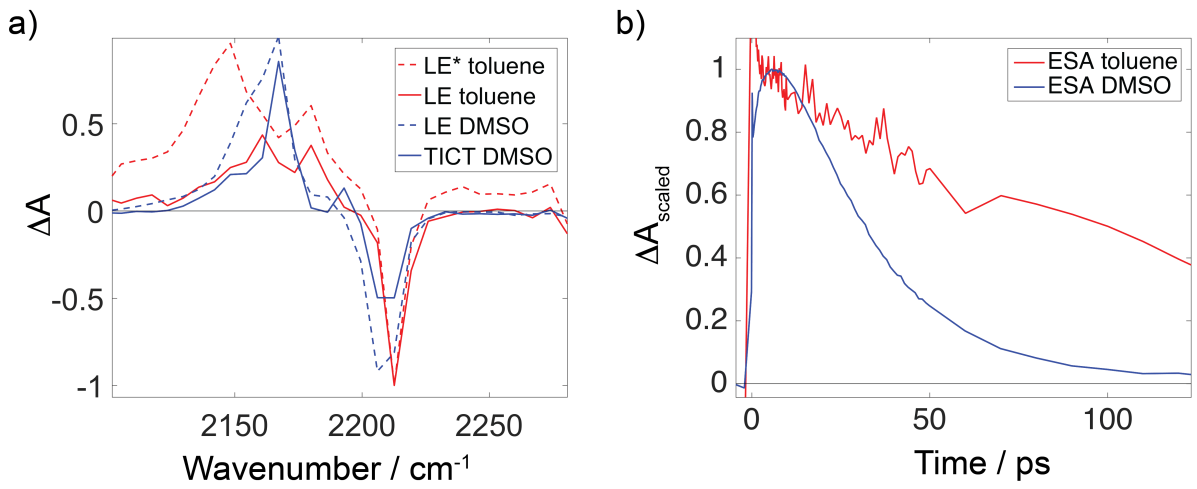

Figure S22: a) Comparison of species associated transient IR spectra in toluene and DMSO. In toluene, hot LE* state relaxes to LE state which decays directly to the ground state. In DMSO, LE state decays to the transient intermediate prior to ground state repopulation, which we assign to TICT formation; b) Characteristic rise attributed to the TICT state formation can be observed in DMSO.

Experimental details

All solvents used were of HPLC grade or spectroscopic grade. DMSO and MeCN were dried over 4 Å molar sieves and passed through activated Al_2O_3 before use. Toluene was distilled from CaH_2 prior to use and stored over molecular sieves under N_2 atmosphere. EtOAc was stirred with K_2CO_3 for 30 minutes, passed over activated Al_2O_3, distilled and stored over 4 Å molar sieves under N_2 atmosphere. Compound **1** was prepared according to the previously reported procedure.[23]

UV-VIS Steady-State Measurements

All absorption spectra were recorded on a Shimadzu UV-2700 spectrophotometer. Fluorescence excitation and emission spectra were recorded using a SPEX Fluorolog 3-22 fluorimeter, equipped with double grating monochromators in both the excitation and emission channels. The light source used for excitation was a 450 W Xenon lamp and the detector was a Peltier cooled R636-10 (Hamamatsu) photomultiplier tube. All spectra were collected in

right-angle geometry and corrected for the spectral sensitivity of the instrument, and lamp intensity fluctuations.

Time-correlated Single Photon Counting

Fluorescence decay curves of **1** were measured using time-correlated single photon counting (TCSPC). For excitation, we used a tunable Ti:sapphire laser (Chameleon Ultra, Coherent), operating at a repetition rate of 80 MHz, with pulse width of 150 fs. An APE pulse picker was used to reduce the rate to 8 MHz. The excitation wavelength of 488 nm was obtained by frequency doubling (APE SHG unit). The instrument response function (fwhm ∼24 ps) was determined using scattered light at the excitation wavelength from a ceramic plate placed at 45^o. An ORIEL Cornerstone 260 mm monochromator was used with an MCP detector (Hamamatsu R3809U-51). A 488 nm notch filter (placed before the monochromator) was used to block the excitation light. TCSPC histograms were recorded up to $\sim 10^4$ counts in the peak channel, and were fitted using nonlinear least squares with IRF deconvolution using DecFit software[24,25] written in Python by Nikolai Tkachenko (Tampere University of Technology, Finland).

Femtosecond VIS-pump IR-probe Transient Absorption

Tunable visible pump and mid-IR probe were generated using a Ti:sapphire laser (Spectra-Physics Hurricane, 600 μJ pulse). VIS pump pulses at 488 nm were generated by sum-frequency mixing the Ti:sapphire pump and an idler of an OPA in BBO (VIS pulse energy was $\sim 3\mu$J); IR probe pulses were generated by difference-frequency mixing signal and idler from a second OPA in $AgGaS_2$. The sample cell with CaF_2 windows spaced by 500 μm was placed in the IR focus. Using a Newport ESP300 translation stage, the delay positions were scanned by mechanically adjusting the beam path of the VIS pump. A temporal resolution of 200 fs was estimated from the fwhm of the pump-probe cross-correlation function. The transient spectra were obtained by subtracting non-pumped absorption spectra from the

pumped absorption spectra that were recorded by a custom built 30 pixel MCT detector coupled to an Oriel MS260i spectrograph. Target analysis was conducted with Glotaran[26] and Matlab. In all cases, deconvolution with a gaussian shaped temporal IRF was used to obtain the fits.

References

(1) Mataga, N.; Kaifu, Y.; Koizumi, M. Solvent effects upon fluorescence spectra and the dipolemoments of excited molecules. *Bull. Chem. Soc. Jpn* **1956**, *29*, 465–470.

(2) Lakowicz, J. R. *Principles of Fluorescence Spectroscopy, 3rd Ed*; Springer Science & Business Media, 2006.

(3) Arzhantsev, S.; Zachariasse, K. A.; Maroncelli, M. Photophysics of trans-4-(dimethylamino)-4'-cyanostilbene and its use as a solvation probe. *J. Phys. Chem. A* **2006**, *110*, 3454–3470.

(4) Dahl, K.; Biswas, R.; Ito, N.; Maroncelli, M. Solvent dependence of the spectra and kinetics of excited-state charge transfer in three (alkylamino) benzonitriles. *J. Phys. Chem. B* **2005**, *109*, 1563–1585.

(5) Jin, H.; Liang, M.; Arzhantsev, S.; Li, X.; Maroncelli, M. Photophysical characterization of benzylidene malononitriles as probes of solvent friction. *J. Phys. Chem. B* **2010**, *114*, 7565–7578.

(6) Strickler, S.; Berg, R. A. Relationship between absorption intensity and fluorescence lifetime of molecules. *J. Chem. Phys.* **1962**, *37*, 814–822.

(7) Förster, T.; Hoffmann, G. Die viskositätsabhängigkeit der fluoreszenzquantenausbeuten einiger farbstoffsysteme. *Z. Phys. Chem.* **1971**, *75*, 63–76.

(8) Petrowsky, M.; Fleshman, A. M.; Frech, R. Application of the Compensated Arrhenius Formalism to Fluidity Data of Polar Organic Liquids. *J. Phys. Chem. B* **2013**, *117*, 2971–2978.

(9) Suhina, T.; Weber, B.; Carpentier, C. E.; Lorincz, K.; Schall, P.; Bonn, D.; Brouwer, A. M. Fluorescence Microscopy Visualization of Contacts Between Objects. *Angew. Chem. Int. Ed.* **2015**, *54*, 3688–3691.

(10) Haynes, W. M. *CRC Handbook of Chemistry and Physics, 95th Ed.*; CRC press, 2014.

(11) Yanai, T.; Tew, D. P.; Handy, N. C. A new hybrid exchange–correlation functional using the Coulomb-attenuating method (CAM-B3LYP). *Chem. Phys. Lett.* **2004**, *393*, 51–57.

(12) Dreuw, A.; Head-Gordon, M. Single-reference ab initio methods for the calculation of excited states of large molecules. *Chem. Rev.* **2005**, *105*, 4009–4037.

(13) Chai, J.-D.; Head-Gordon, M. Long-range corrected hybrid density functionals with damped atom–atom dispersion corrections. *Phys. Chem. Chem. Phys.* **2008**, *10*, 6615–6620.

(14) Cancès, E.; Mennucci, B.; Tomasi, J. A new integral equation formalism for the polarizable continuum model: Theoretical background and applications to isotropic and anisotropic dielectrics. *J. Chem. Phys.* **1997**, *107*, 3032–3041.

(15) Tomasi, J.; Mennucci, B.; Cammi, R. Quantum mechanical continuum solvation models. *Chem. Rev.* **2005**, *105*, 2999–3093.

(16) Caricato, M.; Mennucci, B.; Tomasi, J.; Ingrosso, F.; Cammi, R.; Corni, S.; Scalmani, G. Formation and relaxation of excited states in solution: A new time dependent polarizable continuum model based on time dependent density functional theory. *J. Chem. Phys.* **2006**, *124*, 124520–124513.

(17) Frisch, M. J.; Trucks, G. W.; Schlegel, H. B.; Scuseria, G. E.; Robb, M. A.; Cheeseman, J. R.; Scalmani, G.; Barone, V.; Mennucci, B.; Petersson, G. A. et al. Gaussian 09 Revision D.01. Gaussian Inc. Wallingford CT 2009.

(18) Becker, W. *Advanced Time-Correlated Single Photon Counting Techniques*; Springer Science & Business Media, 2005; Vol. 81.

(19) Horng, M.-L.; Gardecki, J.; Maroncelli, M. Rotational dynamics of coumarin 153: Time-dependent friction, dielectric friction, and other nonhydrodynamic effects. *J. Phys. Chem. A* **1997**, *101*, 1030–1047.

(20) Rettig, W. Intramolecular rotational relaxation of compounds which form "twisted intramolecular charge transfer" (TICT) excited states. *J. Phys. Chem.* **1982**, *86*, 1970–1976.

(21) Golub, G. H.; Reinsch, C. Singular value decomposition and least squares solutions. *Numer. Math.* **1970**, *14*, 403–420.

(22) van Stokkum, I. H.; Larsen, D. S.; van Grondelle, R. Global and target analysis of time-resolved spectra. *BioChim. Biophys. Acta, Bioenerg.* **2004**, *1657*, 82–104.

(23) Gubler, U.; He, M.; Wright, D.; Roh, Y.; Twieg, R.; Moerner, W. Monolithic photorefractive organic glasses with large coupling gain and strong beam fanning. *Adv. Mater.* **2002**, *14*, 313–317.

(24) Lehtivuori, H.; Efimov, A.; Lemmetyinen, H.; Tkachenko, N. V. Distributed decay kinetics of charge separated state in solid film. *Chem. Phys. Lett.* **2007**, *437*, 238–242.

(25) Lehtivuori, H.; Kumpulainen, T.; Efimov, A.; Lemmetyinen, H.; Kira, A.; Imahori, H.; Tkachenko, N. V. Photoinduced Electron Transfer in Langmuir- Blodgett Monolayers of Double-Linked Phthalocyanine- Fullerene Dyads. *J. Phys. Chem. C* **2008**, *112*, 9896–9902.

(26) Snellenburg, J.; Laptenok, S.; Seger, R.; Mullen, K.; Van Stokkum, I. Glotaran: a Java-based graphical user interface for the R package TIMP. *J. Stat. Softw.* **2012**, *49*.